

## SPOT LIGHT SAR IMAGE AUTOFOCUS USING MINIMUM ENTROPY CRITERION

<sup>1</sup>G Roopa Krishna Chandra,<sup>2</sup>Katta Mahesh Babu,<sup>3</sup>Vukoti Joshi,<sup>4</sup>Gandi Hemanth<sup>1</sup>Assistant Professor, Department of Electronics & communication engineering, Andhra Loyola Institute of Engineering And Technology, Vijayawada, India.<sup>2,3,4</sup>UG students, Department of Electronics & communication engineering, Andhra Loyola Institute of Engineering And Technology, Vijayawada, India.<sup>(1</sup>roopakrishnassp@gmail.com,<sup>2</sup>kattamahesh.864@gmail.com,<sup>3</sup>joshivukoti@gmail.com,<sup>4</sup>Ghdpavankumar@gmail.com)

**Abstract**-An optimization algorithm of minimum entropy-based autofocus is presented for SAR (synthetic aperture radar) imaging. Entropy is used to measure the focus quality of the image, and better focus corresponds to smaller entropy. The technique which starts with a complex image domain, based on blind DE convolution using minimum entropy criteria, carries out phase error correction by global search. In the paper, according to R-D (Range-Doppler) algorithm, phase errors are corrected by using minimum entropy criteria for SAR imaging. The simulating results show the validity of the technique to improve the imaging quality.

**Keywords**-SAR Imaging; Autofocus; Minimum Entropy; Phase Error.

## I. INTRODUCTION

The SAR (synthetic aperture radar) represents a turning point in the history of radar technology [1]. We know that SAR images not only show fixed targets and moving targets, but also acquire high-resolution images in extremely difficult weather conditions. There are three models based on the beam scanning system: the SAR band-map, the SAR reflector, and the scanning SAR. The SAR of the band map has the fixed direction of the light beam and the aircraft. The beam scan is parallel to the area of the airplane track band and acquires the radar image. It can also be divided into SARs with a lateral appearance and squinting eyes. In the SAR reflector, the radar beam that points to the scene of the images in the time of accumulation of the synthetic aperture, can be a prolonged observation of the scene, to obtain the length of the synthetic aperture, and therefore obtain a high-resolution azimuth. This mode is suitable for small scenes and high resolution detailed analysis of the image application environment. The scan SAR, the radius indicating the flight direction of the aircraft can vary and can be explored by skipping different areas of the band, but it can also be a longer time point for certain scenes. It is the combination of the SAR travel map and the SAR goal.

The SAR motion compensation technology is one of the key technologies of SAR images [2, 3]. It is the premise of the SAR image algorithm. With the continuous improvement of the image resolution, the requirement of precision of the compensation of the movement between the phase center of the antenna and the objective of the images is increased. Although the SAR system is equipped with advanced navigation equipment, in terms of synthetic opening time, it is not easy to accurately track the position of the aircraft. Moreover, it will generate a phase error of the approximation of the image algorithm and of the effects of atmospheric propagation and will cause the blurring of the image at high resolution which causes the deterioration of the

image. Therefore, to obtain a well-focused image, after the compensation of the conventional movement, high resolution images of the raw SAR data are often required, to estimate and automatically compensate the residual phase error, this process is called autofocus.

It is known that autofocusing methods commonly use Map Drift (MD) [4] and Phase Gradient Autofocus (PGA). MD could estimate the quadratic phase errors caused by the unstable operator's platform speed and compensate completely. See Figure 1. It has a computational load so heavy that MD cannot adapt to the high-resolution image. The PGA algorithm does not need to estimate the order of phase errors, which is suitable for correcting the higher order error. A broadband technique, such as the combined filter technique, the stretching technique, or the step-by-step screening technique, is generally used to improve the resolution of the range. Thus, signals scattered with different azimuths resolve to use their differences in slow time. Clutter blocking, range correction and focus are used to improve azimuth resolution. This document presents an improved algorithm to implement the automatic image optimization approach. Entropy is used to measure the quality of the image focus. A better approach results in less entropy. The minimum entropy algorithm is different from MD and PGA, which starts from the complex image domain and appears several times for the best parameter. Some results of this document have been delivered in.

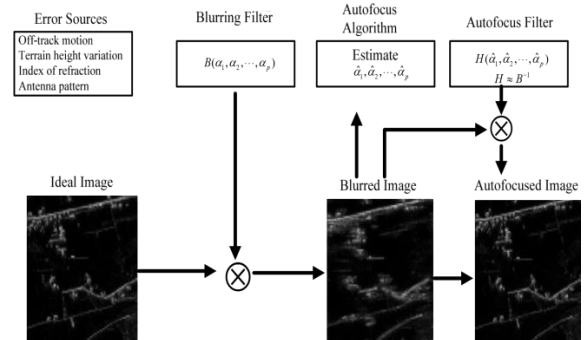


Figure 1. SAR autofocus algorithm

## II. SYSTEM MODEL

Consider a highlighted target region composed of a series of stationary targets located in the coordinates  $(x_n, y_n)$  ( $n = 1, 2, \dots$ ) in Figure 2, the illuminated target area is inclined  $(X_c, Y_c)$ . The radar illuminates the target area with the  $p(t)$  signal. The radar signal is limited by the band within the fast time frequency region.

$$\omega \in [\omega_c - \omega_0, \omega_c + \omega_0] = [\omega_{\min}, \omega_{\max}] \quad (1)$$

Where  $w_{\min}$ ,  $w_{\max}$  are the minimum and maximum frequencies of fast radar signal time.

The synthetic opening domain  $u$  is formed by the movement of the radar that carries an aircraft along a line parallel to the  $y$  axis. The measurements of the synthetic aperture are made at discrete values of  $u$  which are separated by

$$\Delta u = \frac{v_r}{PRF} \tag{2}$$

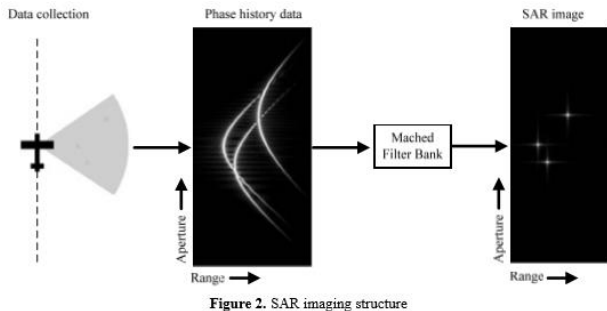


Figure 2. SAR imaging structure

Where  $v_r$  is the plane speed and PRF is the pulse repetition rate (i.e. the number of pulses transmitted per second) of the radar. The size of the synthetic opening is made inside a finite aperture where  $2L$  is the length of the synthetic aperture.

To simplify the annotations, we begin our analysis by considering the acquired SAR signal, a fixed frequency of fast time and slow time or in the synthetic aperture,

$$s(\omega, u) = P(\omega) \sum_n a_n(\omega, x_n, y_n - u) h_s(\omega, u; x_n, y_n) \tag{3}$$

$$= P(\omega) \sum_n a_n(\omega, x_n, y_n - u) a_s(\omega, u; x_n, y_n) \exp[-j2k\sqrt{x_n^2 + (y_n - u)^2}]$$

III. PHASE ERROR EFFECT OF THE IMAGING

In the history of the stray SAR signal, the azimuth echoes of the ideal target point take the form of a chirp signal. The high resolution of the azimuth of the SAR system is obtained by compressing the pulses. In fact, due to the measurement error of position and movement, the approximation of the image algorithm, the limits of hardware performance and the effect of atmospheric transmission, the azimuth SAR to the echo is no longer the standard FM linear signal. The phase error will be reported to eliminate the residual phase of the components of the standard linear FM signal. The phase error can be divided into a low frequency phase error, a high frequency sinusoidal phase error and a wide band phase error. Its effects on the image are shown in Table 1.

Phase error category	Effect of the image
Low-frequency phase error	Geometric distortion,
High frequency sine phase error	resolution loss
Wideband phase error	Contrast decline, false target
	SNR reduce

Table 1. Phase error and effect

The high frequency sinusoidal phase error occurs when compensating for antenna phase centre vibrations (APC). Its impact on the image to produce paired echoes, which leads to a false target appears. The broadband phase error generated by measurement errors in random motion affects the contrast of the image. The high frequency sinusoidal phase error and the broadband phase error belong to a high frequency phase error. In modern SAR systems, through the inertial measurement unit (IMU) combined with the Global Positioning System (GPS), it is possible to determine the movement structure of the APC and other high-frequency movements. Therefore, in the movement compensation phase, the high frequency phase error can be better compensated. Subsequently, the use of different auto-focus

algorithms is mainly directed against the low frequency phase error without compensation.

The low frequency phase error is mainly due to errors in measuring the speed and acceleration of the SAR motion sensor and to the phase error inherent in the image algorithm which cannot be completely compensated at the echo date, as the correction of incomplete distance bending and planar movement. The low frequency phase error includes a linear phase error, the quadratic phase error and the upper phase error. The linear phase error can be expressed as:

$$\Delta\phi_e(t) = 2\pi f_{e1}t \quad |t| \leq \frac{T_s}{2} \tag{1}$$

Where  $f_{e1}$  is the linear phase error coefficient. In the isolated point lens, the linear phase error caused the lens to shift. In the distribution objectives, if the linear phase errors of the frequency of all the target points are equal, the linear phase error caused the displacement of the entire image. If the dot point  $f_{e1}$  is not equal, ie the variant of the space, it would cause the imaginary distortion of the image.

The quadratic phase error can be expressed as:

$$\Delta\phi_e(t) = \pi f_{e2}t^2 \quad |t| \leq \frac{T_s}{2} \tag{2}$$

Where  $f_{e2}$  is the quadratic phase error coefficient. So the signal of azimuthal echoes can be expressed as:

$$s(t) = \exp[j\pi(k + k_e)t^2] \quad |t| \leq \frac{T_s}{2} \tag{3}$$

Equation (3) shows that the presence of a quadratic phase error is equivalent to changing the rate of squeaks of the Doppler echo signal, and does not match the adapted filter, which produces a blur. The error of the cubic phase can be expressed as:

$$\Delta\phi_e(t) = \pi f_{e3}t^3 \quad |t| \leq \frac{T_s}{2} \tag{4}$$

Where  $f_{e3}$  is the quadratic phase error coefficient. The error of the cubic phase so that the impulse response of the system to produce a lobe level of the symmetrical lateral lobe is increased, causing deterioration of the image contrast. The cubic phase error caused the asymmetrical lateral lobe for the system impulse response. The increase in the level of a side lobe has led to the deterioration of the contrast of the images.

IV. MINIMUMENTROPYAUTOFOCUS TECHNIQUE

Most of the autofocus algorithm used to eliminate the constant empty phase error. This type of error in the image of the influence of all dispersion points is the same. Therefore, the blurring of the SAR image can be seen as the point dispersion function of the convolution results caused by a clear image and a phase error. As shown in Figure 3. Image of the blurred fuzzy point scatter image function.

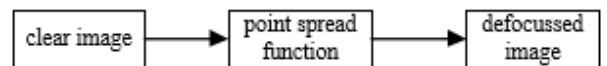


Fig.3: Image defocusing equivalent model.

According to the previous model, the autofocus algorithm due to the impulse response of the system, this is a typical problem of blind convolution solution. Shalvi and Weinstein have shown that using the convolution of the blind solution criterion of minimal entropy in most conditions can converge the correct result. The condition of the premise is to request that the data do not obey the Gaussian distribution and the transmission function is not zero.

Raw SAR signal data is combined by many independent scattered echoes. The SAR image reflects the objective dispersion coefficient of the image. For unit resolution, because the amplitude and phase of the echo signal are random after the amplitude synthesis is a random variable, and their characteristics and dimensions of unitary resolution and carrier frequency and so on statistics. In case of high resolution, each resolvable diffuser body unit number is limited, the law of large numbers is not set, therefore, the dispersion coefficient resolver is non-Gaussian distribution. But we have little prior knowledge of the transmission function. Therefore, we obtain a minimum entropy criterion to implement the convolution looking at this document, that is, we assume a model error and then in the estimated range, we look for the minimum entropy. This form is not very rigorous in theory, but it is a feasible design scheme, the results of the simulation and the processing of the measured data demonstrated the feasibility of the proposed algorithm.

The minimal entropy autofocus algorithm begins with a complex phase SAR degradation image, which means that it has nothing to do with the type of image algorithm, the inverse Fourier transform bearing to the domain of the remote compression phase history. Complete algorithmic processes as shown in Figure 4.

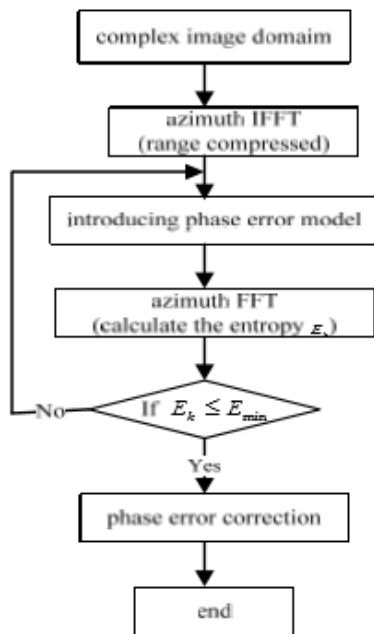


Figure 4. Minimum entropy autofocus algorithm procedure

Due to the linear phase error caused only the general translation of the image, without the influence of the image structure, so in the domain of the history of remote compression, but reasonable to assume that phase error model.

$$\Delta\phi_e(t) = \alpha t^2 + \beta t^3 + \gamma t^4 + \dots \tag{5}$$

For M by N pixels image area S, Shannon entropy definition is given by

$$E(S) = -\sum_m \sum_n \rho(m,n) \log \rho(m,n)$$

$$\rho(m,n) = \frac{|S(m,n)|^2}{P}$$

$$P = \sum_m \sum_n |S(m,n)|^2 \tag{6}$$

According to Shannon's definition of entropy, the entropy of the image has the following properties: (1) The invariance of the scale, ie the brightness has nothing to do with the entropy of the image; (2) substitution invariance, that is, the entropy has nothing to do with the position of the pixel distribution; (3) The weak overlap. When the SAR image is better focused, the sharpest peak and the entropy of the image are smaller. Therefore, when the entropy of the image is reduced to a minimum, the focusing effect is better and the Doppler parameter is the most precise.

V. SIMULATION RESULTS AND ANALYSIS

5.1 Simulation For Point Target

Here give the simulation results. For nine points targets, we suppose radar transmits LFM signals, and give the simulation parameters in Table 2.

Parameter	Value	Parameter	Value
Wavelength	3cm	Imaging process time (T <sub>i</sub> )	200 ms
Pulse width (T <sub>p</sub> )	4us	PRF (F <sub>pr</sub> )	2000 Hz
Pulse bandwidth (B)	20 MHz	Velocity(v)	600 m/s
Scenario center range (R <sub>0</sub> )	8000 m	Angle LOS with azimuth	25°

Table.2: Radar characteristics and parameters.

Since high-order components in the low-frequency phase error are generally smaller and have little effect on the main lobe, then it can reasonably be assumed that the phase error contains error 2 and 3 times and Figure 5 shows the calculation methods and the minimum entropy.

$$\Delta\phi_e(t) = \alpha t^2 + \beta t^3 \tag{7}$$

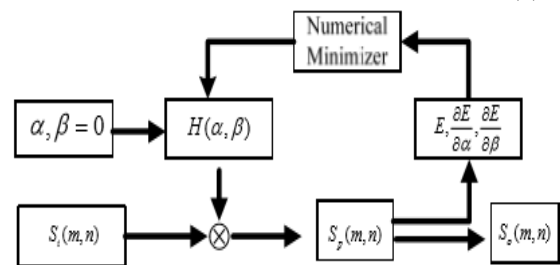
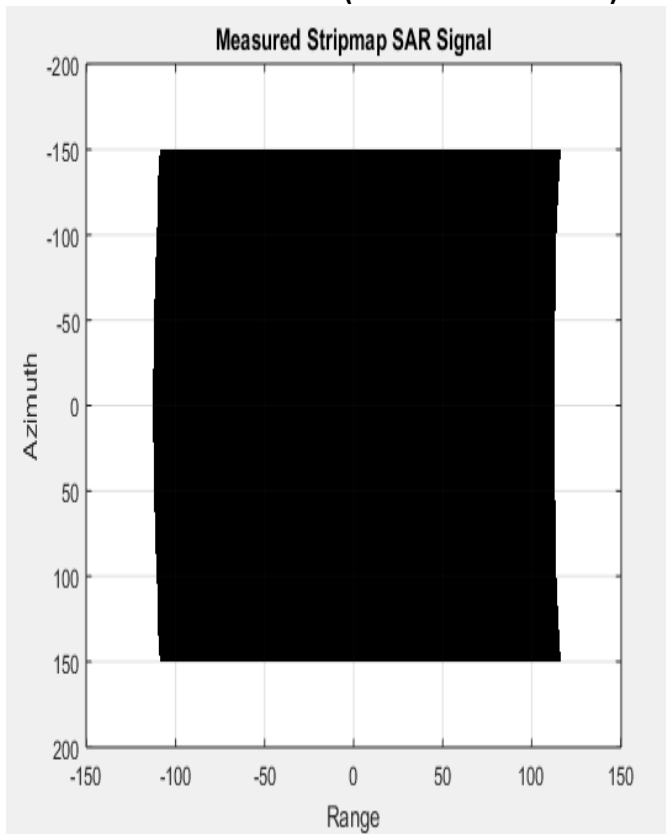


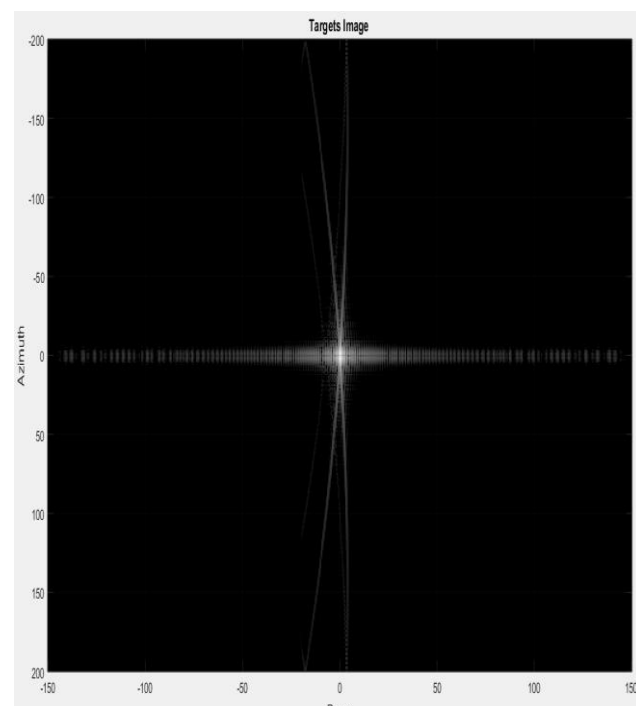
Figure 5. Minimum entropy calculation

Figure 6 (a) shows the original image of the point target given by the Doppler interval algorithm and presents a severe blur in the direction of the azimuth. In fact, the quadratic phase error coefficient reflects the deviation of the aircraft speed. As a result, we can estimate the approximate range of. The phase error of order higher than more cubic is generally less than the quadratic phase error, therefore it is possible to determine the interval of the phase error coefficient. Figure 6 (b) is the image with automatic focusing of minimum entropy. The results show that it is effective to improve the quality of the reflector SAR images through the technique.

the theoretical analysis and the processing results of the measured SAR data demonstrated the efficacy of this technique. Furthermore, this document provides an optimized perspective for autofocus, which is important for SAR images.



(a)



(b)

Fig.6: SAR imaging with point target: (a) original image, (b) image with the minimum-entropy autofocus.

## VI. CONCLUSION

In this document an autofocus method with minimal optimized entropy was presented. Phase errors can be accurately estimated through the constructed phase error coefficient. Both

## REFERENCES

- [1] H. M. J. Cantalloube and C. E. Nahum, "Multiscale Local Map-Drift-Driven Multilateration SAR Autofocus Using Fast Polar Format Image Synthesis", *IEEE Transactions on Geoscience and Remote Sensing*, vol. 49, pp. 3730-3736, 2011.
- [2] L. Kuang-Hung and D. C. Munson, "Fourier-Domain Multichannel Autofocus for Synthetic Aperture Radar", *IEEE Transactions on Image Processing*, vol. 20, pp. 3544-3552, 2011.
- [3] L. Lijuan, B. Xia, Z. Juan, and T. Ran, "SAR Autofocus Using Wiener Deconvolution," in *Pervasive Computing Signal Processing and Applications (PCSPA) on The First International Conference*, pp. 1256-1259, 2010.
- [4] R. L. Morrison, M. N. Do and D. C. Munson, "MCA: A Multichannel Approach to SAR Autofocus", *IEEE Transactions on Image Processing*, vol. 18, pp. 840-853, 2009.
- [5] M. Z. A. Bhotto and A. Antoniou, "A new normalized minimum-error entropy algorithm with reduced computational complexity," in *Circuits and Systems on IEEE International Symposium*, pp. 2561-2564, 2009.
- [6] Y. Yaming, "On the Entropy of Compound Distributions on Nonnegative Integers", *IEEE Transactions on Information Theory*, vol. 55, pp. 3645-3650, 2009.
- [7] S. Aviyente and W. J. Williams, "Minimum entropy time-frequency distributions," *Signal Processing Letters, IEEE*, vol. 12, pp. 37- 40, 2005.
- [8] D. Erdogmus and J. C. Principe, "An error-entropy minimization algorithm for supervised training of nonlinear adaptive systems", *IEEE Transactions on Signal Processing*, vol. 50, pp. 1780-1786, 2002.
- [9] Xu Feng, Wang Xia, Zheng Xiao-Dong, Wang Hao, "An Adaptive Compressed Sensing Method in Speech", *IJACT*, Vol. 4, No. 8, pp. 36 ~ 43, 2012.
- [10] Yong CHEN, "The Study on Nonlinear Signal Processing based on Particular Algorithm", *IJACT*, Vol. 4, No. 16, pp. 320 ~ 328, 2012.
- [11] Hongbing Sun, Shenfeng Yuan, Xia Zhao, Henbao Zhou, Dong Liang, "Technology of structure damage monitoring based on multiagent", *Journal of Systems Engineering and Electronics*, Vol.21, No.4, pp.616-622, 2010.
- [12] SUN Hong-bing, YUAN Shenfeng, LIANG Dong, YANG Weibo, "Technology of Distributed Structural Health Monitoring System with Multi-layer and Multi-Agent", *IJACT: International Journal of Advancements in Computing Technology*, Vol. 3, No. 10, pp. 274 ~ 282, 2011.